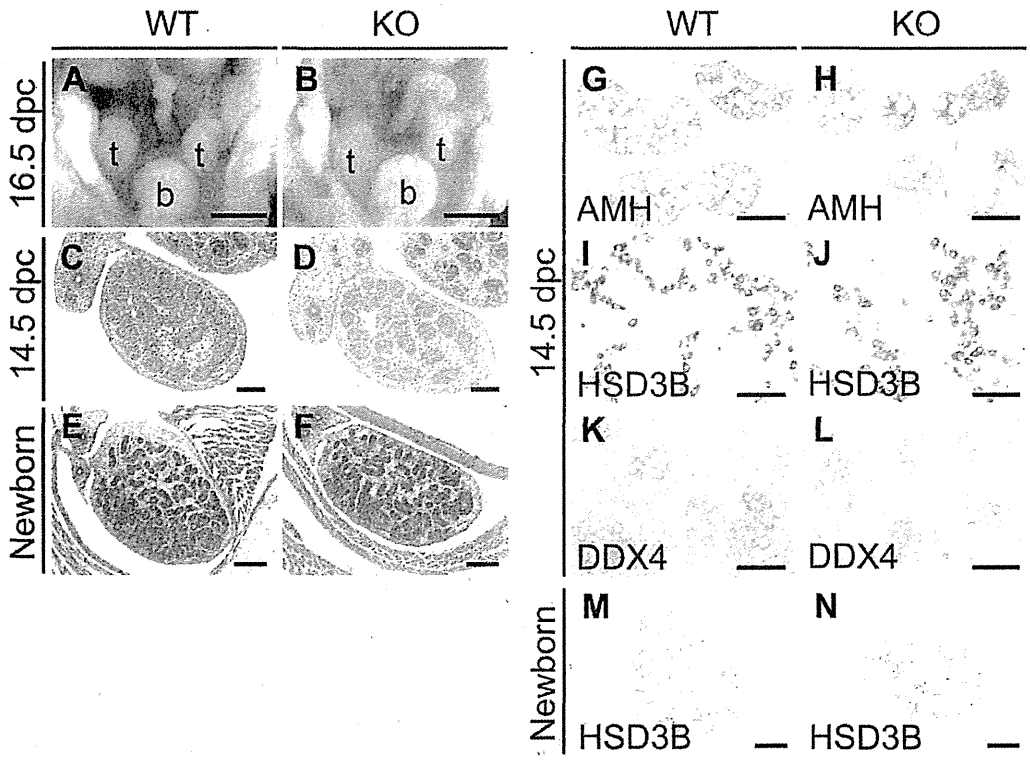

FIG. 5. Internal genitalia of WT and *Mamld1* KO male mice. A and B, Appearance of internal genital organs at 16.5 dpc. C–F, Histological findings of testes at 14.5 dpc and birth. G–N, Immunohistochemical findings of testes at 14.5 dpc and birth. b, Bladder; t, testis. *Scale bars*: 1 mm (A and B), 100 μm (C and D), 200 μm (E, F, M, and N), and 50 μm (G–L).

Discussion

The *Mamld1* mRNA expression was gradually and steadily increased from 12.5 to 18.5 dpc in the fetal testis of WT male mice. In this regard, intratesticular T has also been reported to increase in a similar manner in the mouse (10, 11). In addition, human study has also revealed clear *MAMLD1* expression in the fetal testis. These findings would argue for a positive role of *MAMLD1/Mamld1* in the T production in the fetal testis (1, 21).

We generated and studied *Mamld1* KO male mice. The results are summarized as follows: 1) mRNA levels of genes exclusively expressed in Leydig cells (*Star*, *Cyp11a1*, *Cyp17a1*, *Hsd3b1*, and *Insl3*) were mildly but significantly reduced, whereas those of genes expressed in other cell types or in Leydig and other cell types grossly remained normal (*Hsd17b3* is expressed in Sertoli cells of the fetal testis, although it is expressed in Leydig cells of the adult testis) (22, 23); 2) despite such mild reduction of mRNA levels, CYP17A1 and HSD3B proteins were sufficiently produced; 3) no demonstrable abnormality was identified by detailed studies for the external and internal genital regions; and 4) the *Mamld1* KO male mice retained normal fertility. Collectively, these findings imply that *Mamld1* deficiency reduces mRNA expression levels of multiple, if not all, genes expressed in mouse fetal Leydig cells but permits normal genital development and reproductive function. In support of this notion, such discrepancy between mRNA levels and protein levels as well as phenotypic consequences has been reported previously (24–26). Indeed, Greenbaum *et al.* (27) have proposed three possible explanations for the poor correlations between mRNA and protein expression levels: 1) there are many complicated and varied posttranscriptional mechanisms involved in turning mRNA into protein that are not yet sufficiently well defined; 2) proteins may differ substantially in their *in vivo* half lives; and 3) there may be a significant amount of error and noise in both protein and mRNA experiments that limit our ability to get a clear picture. These explanations would also apply to our results indicating normal expression of CYP17A1 and HSD3B proteins, in the presence of mildly but significantly reduced expression of *Cyp17a1* and *Hsd3b1* mRNAs. Furthermore, because CYP17A1 and HSD3B protein levels increased in a manner grossly similar to that reported for intratesticular T (10, 11) in both the *Mamld1* KO male mice and their WT littermates, this would be consistent with the apparently normal testicular function of the *Mamld1* KO male mice.

The normal phenotype in the *Mamld1* KO male mice is contrastive to the DSD phenotype in the *MAMLD1* mu-

TABLE 2. Cross-mating experiments for *Mamld1*

Offspring produced by cross-mating between *Mamld1* KO male mice (n = 5) and WT female mice (n = 24)					
Sex and *Mamld1* genotype	Male (−)	Male (+)	Female (−/−)	Female (+/−)	Female (+/+)
Number and frequency	n/o	89 (45.6%)	n/o	106 (54.4%)	n/o
Offspring produced by cross-mating between *Mamld1* KO male mice (n = 14) and heterozygous female mice (n = 49)					
Sex and *Mamld1* genotype	Male (−)	Male (+)	Female (−/−)	Female (+/−)	Female (+/+)
Number and frequency	84 (23.6%)	96 (27.0%)	94 (26.4%)	82 (23.0%)	n/o
Offspring produced by cross-mating between WT male mice (n = 6) and WT female mice (n = 12)					
Sex and *Mamld1* genotype	Male (−)	Male (+)	Female (−/−)	Female (+/−)	Female (+/+)
Number and frequency	n/o	58 (59.8%)	n/o	n/o	39 (40.2%)
Offspring produced by cross-mating between WT male mice (n = 9) and heterozygous female mice (n = 46)					
Sex and *Mamld1* genotype	Male (−)	Male (+)	Female (−/−)	Female (+/−)	Female (+/+)
Number and frequency	86 (25.3%)	85 (25.0%)	n/o	84 (24.7%)	85 (25.0%)

WT or +, WT; KO or −, *Mamld1* KO; n/o, not obtained.

tation positive patients (1, 3). In this regard, it is notable that male genital development is primarily induced by testicular T that is produced via Δ^5-pathway under the stimulation of chorionic gonadotropin during the first trimester in the human (28–31), whereas it is primarily carried out by testicular T that is produced via Δ^4-pathway independently of the chorionic gonadotropin stimulation during the late gestational period in the mouse (10, 31, 32). Thus, although the detailed mechanism(s) remains to be clarified, such species difference in the fetal male sex development may underlie the phenotypic difference between the *Mamld1* KO male mice and the *MAMLD1* mutation positive patients. In addition, the bias that individuals with abnormal phenotypes only are usually examined in the human study may also be relevant to this matter.

The results of mRNA expression levels and intratesticular hormone concentrations in the *Mamld1* KO male mice are different from those identified by transient *Mamld1* knockdown experiments using siRNAs and MLTCs (6, 8), although the normal Leydig cell number of the *Mamld1* KO male mice appears to be consistent with the sustained proliferation of siRNA-transfected MLTCs (8). Indeed, *Mamld1* knockdown has predominantly affected *Cyp17a1* expression (8) and significantly decreased T and other steroid metabolite after 17α-hydroxylation (6, 8). However, MLTCs are derived from adult Leydig tumor cells and are characterized by a markedly low 17α-hydroxylase activity and a well-preserved 17/20 lyase activity for both Δ^4- and Δ^5-pathways (33). Such unique properties of MLTCs may be relevant to the preferential impairment of *Cyp17a1* expression and 17α-hydroxylation in siRNA-transfected MLTCs.

Two findings also appear to be worth pointing out in this study. First, *Insl3* mRNA expression was significantly reduced and *Amh* mRNA expression was grossly normal, in the *Mamld1* KO mice. Such mRNA expression patterns, if they also take place in the human, would be relevant to the frequent occurrence of cryptorchidism and the lack of müllerian derivatives in patients with *MAMLD1* mutations (1). Second, *Mamld1* KO male mice, WT male mice, homozygous (−/−) female mice, heterozygous (+/−) female mice, and WT female mice were born with frequencies consistent with the Mendelian mode of inheritance. Thus, although *Mamld1* is ubiquitously expressed with strong expressions in the central nervous system (1), *Mamld1* deficiency is unlikely to affect viability.

In summary, the present study implies that *Mamld1* enhances mRNA expression levels of multiple genes exclusively expressed in fetal Leydig cells, although the effects of *Mamld1* deficiency are insufficient to compromise the genital and reproductive development. Further studies will permit a better clarification of the biological function of *MAMLD1/Mamld1*.

Acknowledgments

Address all correspondence and requests for reprints to: Professor Tsutomu Ogata, Department of Pediatrics, Hamamatsu University School of Medicine, Hamamatsu 431-3192, Japan. E-mail: tomogata@hama-med.ac.jp.

This work was supported by the National Center for Child Health and Development Grant 23A-1; Grant for Research on Intractable Diseases from the Ministry of Health, Labor, and

Welfare; Environment Research and Technology Development Fund C-0905 of the Ministry of Environment; Grants-in-Aid for Scientific Research (B) 23390249 and (S) 22227002 and for Young Scientists (B) 24790303 from the Japan Society for the Promotion of Science; and Grant-in-Aid for Scientific Research on Innovative Areas 22132004 from the Ministry of Education, Culture, Sports, Science, and Technology.

Disclosure Summary: The authors have nothing to disclose.

References

1. Fukami M, Wada Y, Miyabayashi K, Nishino I, Hasegawa T, Nordenskjöld A, Camerino G, Kretz C, Buj-Bello A, Laporte J, Yamada G, Morohashi K, Ogata T 2006 CXorf6 is a causative gene for hypospadias. Nat Genet 38:1369–1371
2. Kalfa N, Liu B, Klein O, Ophir K, Audran F, Wang MH, Mei C, Sultan C, Baskin LS 2008 Mutations of CXorf6 are associated with a range of severities of hypospadias. Eur J Endocrinol 159:453–458
3. Ogata T, Laporte J, Fukami M 2009 MAMLD1 (CXorf6): a new gene involved in hypospadias. Horm Res 71:245–252
4. Chen Y, Thai HT, Lundin J, Lagerstedt-Robinson K, Zhao S, Markljung E, Nordenskjöld A 2010 Mutational study of the MAMLD1-gene in hypospadias. Eur J Med Genet 53:122–126
5. van der Zanden LF, van Rooij IA, Feitz WF, Franke B, Knoers NV, Roeleveld N 2012 Aetiology of hypospadias: a systematic review of genes and environment. Hum Reprod Update 18:260–283
6. Fukami M, Wada Y, Okada M, Kato F, Katsumata N, Baba T, Morohashi K, Laporte J, Kitagawa M, Ogata T 2008 Mastermind-like domain-containing 1 (MAMLD1 or CXorf6) transactivates the Hes3 promoter, augments testosterone production, and contains the SF1 target sequence. J Biol Chem 283:5525–5532
7. Lin L, Achermann JC 2008 Steroidogenic factor-1 (SF-1, Ad4BP, NR5A1) and disorders of testis development. Sex Dev 2:200–209
8. Nakamura M, Fukami M, Sugawa F, Miyado M, Nonomura K, Ogata T 2011 Mamld1 knockdown reduces testosterone production and Cyp17a1 expression in mouse Leydig tumor cells. PLoS One 6:e19123
9. Hogan B, Beddington R, Costantini F, Lacy E 1994 Manipulating the mouse embryo: a laboratory manual. New York: Cold Spring Harbor Laboratory Press
10. O'Shaughnessy PJ, Baker P, Sohnius U, Haavisto AM, Charlton HM, Huhtaniemi I 1998 Fetal development of Leydig cell activity in the mouse is independent of pituitary gonadotroph function. Endocrinology 139:1141–1146
11. O'Shaughnessy PJ, Baker PJ, Johnston H 2006 The foetal Leydig cell-differentiation, function and regulation. Int J Androl 29:90–95; discussion 105–108
12. Miyagawa S, Satoh Y, Haraguchi R, Suzuki K, Iguchi T, Taketo MM, Nakagata N, Matsumoto T, Takeyama K, Kato S, Yamada G 2009 Genetic interactions of the androgen and Wnt/β-catenin pathways for the masculinization of external genitalia. Mol Endocrinol 23:871–880
13. Suzuki K, Ogino Y, Murakami R, Satoh Y, Bachiller D, Yamada G 2002 Embryonic development of mouse external genitalia: insights into a unique mode of organogenesis. Evol Dev 4:133–141
14. Fatchiyah, Zubair M, Shima Y, Oka S, Ishihara S, Fukui-Katoh Y, Morohashi K 2006 Differential gene dosage effects of Ad4BP/SF-1 on target tissue development. Biochem Biophys Res Commun 341:1036–1045
15. Graham S, Gandelman R 1986 The expression of ano-genital distance data in the mouse. Physiol Behav 36:103–104
16. Kerin TK, Vogler GP, Blizard DA, Stout JT, McClearn GE, Vandenbergh DJ 2003 Anogenital distance measured at weaning is correlated with measures of blood chemistry and behaviors in 450-day-old female mice. Physiol Behav 78:697–702
17. Swan SH, Main KM, Liu F, Stewart SL, Kruse RL, Calafat AM, Mao CS, Redmon JB, Ternand CL, Sullivan S, Teague JL 2005 Decrease in anogenital distance among male infants with prenatal phthalate exposure. Environ Health Perspect 113:1056–1061
18. Haraguchi R, Mo R, Hui C, Motoyama J, Makino S, Shiroishi T, Gaffield W, Yamada G 2001 Unique functions of Sonic hedgehog signaling during external genitalia development. Development 128:4241–4250
19. Miyagawa S, Matsumaru D, Murashima A, Omori A, Satoh Y, Haraguchi R, Motoyama J, Iguchi T, Nakagata N, Hui CC, Yamada G 2011 The role of sonic hedgehog-Gli2 pathway in the masculinization of external genitalia. Endocrinology 152:2894–2903
20. Wilkinson D 1992 *In situ* hybridization: a practical approach. London: Oxford University Press
21. O'Shaughnessy PJ, Baker PJ, Monteiro A, Cassie S, Bhattacharya S, Fowler PA 2007 Developmental changes in human fetal testicular cell numbers and messenger ribonucleic acid levels during the second trimester. J Clin Endocrinol Metab 92:4792–4801
22. Baker PJ, Sha JH, O'Shaughnessy PJ 1997 Localisation and regulation of 17β-hydroxysteroid dehydrogenase type 3 mRNA during development in the mouse testis. Mol Cell Endocrinol 133:127–133
23. O'Shaughnessy PJ, Baker PJ, Heikkilä M, Vainio S, McMahon AP 2000 Localization of 17β-hydroxysteroid dehydrogenase/17-ketosteroid reductase isoform expression in the developing mouse testis-androstenedione is the major androgen secreted by fetal/neonatal leydig cells. Endocrinology 141:2631–2637
24. Lehmann KP, Phillips S, Sar M, Foster PM, Gaido KW 2004 Dose-dependent alterations in gene expression and testosterone synthesis in the fetal testes of male rats exposed to di (n-butyl) phthalate. Toxicol Sci 81:60–68
25. Thompson CJ, Ross SM, Hensley J, Liu K, Heinze SC, Young SS, Gaido KW 2005 Differential steroidogenic gene expression in the fetal adrenal gland versus the testis and rapid and dynamic response of the fetal testis to di(n-butyl) phthalate. Biol Reprod 73:908–917
26. Weisser J, Landreh L, Söder O, Svechnikov K 2011 Steroidogenesis and steroidogenic gene expression in postnatal fetal rat Leydig cells. Mol Cell Endocrinol 341:18–24
27. Greenbaum D, Colangelo C, Williams K, Gerstein M 2003 Comparing protein abundance and mRNA expression levels on a genomic scale. Genome Biol 4:117
28. Flück CE, Miller WL, Auchus RJ 2003 The 17, 20-lyase activity of cytochrome p450c17 from human fetal testis favors the δ5 steroidogenic pathway. J Clin Endocrinol Metab 88:3762–3766
29. Fowler PA, Bhattacharya S, Gromoll J, Monteiro A, O'Shaughnessy PJ 2009 Maternal smoking and developmental changes in luteinizing hormone (LH) and the LH receptor in the fetal testis. J Clin Endocrinol Metab 94:4688–4695
30. Huhtaniemi IT, Korenbrot CC, Jaffe RB 1977 HCG binding and stimulation of testosterone biosynthesis in the human fetal testis. J Clin Endocrinol Metab 44:963–967
31. Scott HM, Mason JI, Sharpe RM 2009 Steroidogenesis in the fetal testis and its susceptibility to disruption by exogenous compounds. Endocr Rev 30:883–925
32. Baker PJ, O'Shaughnessy PJ 2001 Role of gonadotrophins in regulating numbers of Leydig and Sertoli cells during fetal and postnatal development in mice. Reproduction 122:227–234
33. Panesar NS, Chan KW, Ho CS 2003 Mouse Leydig tumor cells produce C-19 steroids, including testosterone. Steroids 68:245–251

Hindawi Publishing Corporation
International Journal of Endocrinology
Volume 2012, Article ID 584807, 8 pages
doi:10.1155/2012/584807

Review Article

Molecular Bases and Phenotypic Determinants of Aromatase Excess Syndrome

Maki Fukami,[1] Makio Shozu,[2] and Tsutomu Ogata[1,3]

[1] *Department of Molecular Endocrinology, National Research Institute for Child Health and Development, 2-10-1 Ohkura, Setagaya, Tokyo 157-8535, Japan*
[2] *Department of Reproductive Medicine, Graduate School of Medicine, Chiba University, 1-8-1 Inohana, Chuo-ku, Chiba City 206-8670, Japan*
[3] *Department of Pediatrics, Hamamatsu University School of Medicine, 1-20-1 Handayama, Higashi-ku, Shizuoka, Hamamatsu 431-3192, Japan*

Correspondence should be addressed to Maki Fukami, mfukami@nch.go.jp

Received 9 July 2011; Revised 22 September 2011; Accepted 2 October 2011

Academic Editor: Rodolfo Rey

Aromatase excess syndrome (AEXS) is a rare autosomal dominant disorder characterized by gynecomastia. This condition is caused by overexpression of *CYP19A1* encoding aromatase, and three types of cryptic genomic rearrangement around *CYP19A1*, that is, duplications, deletions, and inversions, have been identified in AEXS. Duplications appear to have caused *CYP19A1* overexpression because of an increased number of physiological promoters, whereas deletions and inversions would have induced wide *CYP19A1* expression due to the formation of chimeric genes consisting of a noncoding exon(s) of a neighboring gene and *CYP19A1* coding exons. Genotype-phenotype analysis implies that phenotypic severity of AEXS is primarily determined by the expression pattern of *CYP19A1* and the chimeric genes and by the structural property of the fused exons with a promoter function (i.e., the presence or the absence of a natural translation start codon). These results provide novel information about molecular mechanisms of human genetic disorders and biological function of estrogens.

1. Introduction

Aromatase encoded by *CYP19A1* is a cytochrome P450 enzyme that plays a key role in estrogen biosynthesis [1]. It catalyzes the conversion of Δ^4-androstendione into estrone (E_1) and that of testosterone (T) into estradiol (E_2) in the placenta and ovary as well as in other tissues such as the fat, skin, bone, and brain [1].

Overexpression of *CYP19A1* causes a rare autosomal dominant disorder referred to as aromatase excess syndrome (AEXS, OMIM no. 139300) [2–8]. AEXS is characterized by pre- or peripubertal onset gynecomastia, gonadal dysfunction, advanced bone age from childhood to pubertal period, and short adult height in affected males [2–8]. In particular, gynecomastia is a salient feature in AEXS, and, therefore, this condition is also known as hereditary gynecomastia or familial gynecomastia [5]. Affected females may also show several clinical features such as macromastia, precocious puberty, irregular menses, and short adult height [5, 6, 8].

Recently, three types of cryptic genomic rearrangements around *CYP19A1* have been identified in 23 male patients with AEXS [2–4]. The results provide useful implications not only for the clarification of underlying mechanisms but also for the identification of phenotypic determinants. Here, we review the current knowledge about AEXS.

2. The Aromatase Gene (*CYP19A1*)

CYP19A1 encoding aromatase is located on 15q21.2 adjacent to *DMXL2* and *GLDN* (Figure 1) [3, 9]. It spans ~123 kb and consists of at least 11 noncoding exons 1 and nine coding exons 2–10 [9–12]. Each exon 1 is accompanied by a tissue-specific promoter and is spliced alternatively onto a common splice acceptor site at exon 2, although some transcripts are known to contain two of the exons 1 probably due to a splice error [9–11]. Transcription of *CYP19A1* appears to be tightly regulated by alternative usage of the multiple

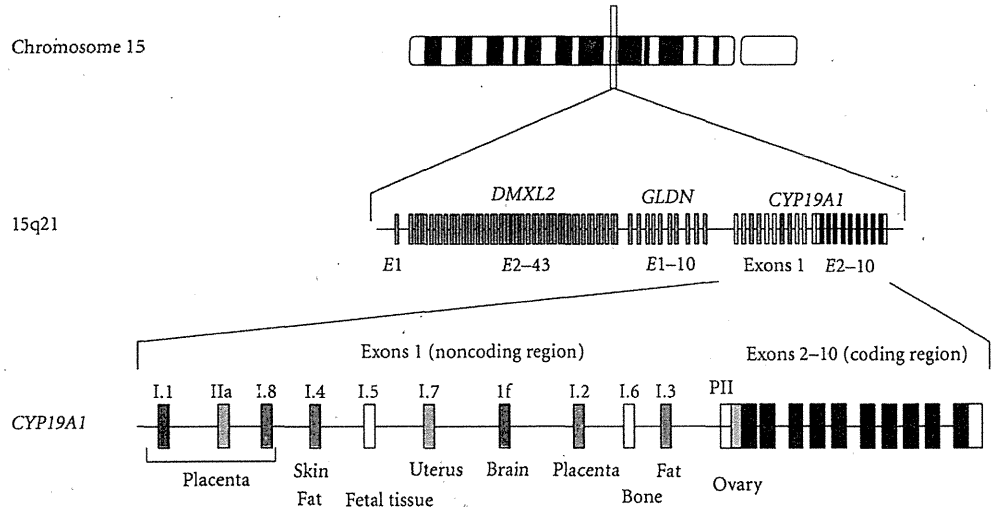

FIGURE 1: Simplified schematic representation indicating the genomic structure of *CYP19A1*. *CYP19A1* is located on 15q21.2 adjacent to *DMXL2* and *GLDN* and consists of at least 11 noncoding exons 1 and nine coding exons 2–10 [9, 10]. Each exon 1 is accompanied by a tissue-specific promoter and is spliced alternatively onto a common splice acceptor site at exon 2 [9–13].

promoters [9–13]. Actually, *CYP19A1* is strongly expressed in the placenta and moderately expressed in the ovary, whereas it is only weakly expressed in a rather limited number of tissues including skin, fat, and hypothalamus [4, 13]. Of the 11 noncoding exons 1, exon I.4 seems to play a critical role in the regulation of estrogen biosynthesis in males, because this exon contains the major promoter for extragonadal tissues [9, 10].

3. Molecular Bases of AEXS

A family with dominantly transmitted gynecomastia of prepubertal onset was first described in 1962 by Wallach and Garcia [14]. After this initial report, several cases have been described [5–8, 15]. Laboratory examinations of the affected males revealed markedly elevated serum estrogen values and estrogen/androgen ratios and significantly increased aromatase activity in fibroblasts and lymphocytes [5–8, 15]. Linkage analyses in two families indicated a close association between *CYP19A1*-flanking polymorphic markers and the disease phenotype [5, 6]. Thus, the condition was assumed to be caused by gain-of-function mutations of *CYP19A1*, and, therefore, the name of AEXS was coined for this condition [7, 8]. However, since direct sequencing and Southern blotting analysis failed to detect mutations or copy number abnormalities in the coding region of *CYP19A1* [5, 6], the molecular basis of this entity remained elusive until recently.

In 2003, Shozu et al. reported a father-son pair and a sporadic case with AEXS in whom they identified heterozygous chromosomal inversions of the chromosome 15 [2]. Subsequently, Demura et al. performed detailed molecular studies for these cases and additional two cases and characterized four types of inversions affecting the 5′ region of *CYP19A1* [3]. Each inversion has resulted in the formation of a chimeric gene consisting of *CYP19A1* coding exons and exon 1 of the widely expressed neighboring genes, that is, *CGNL1*, *TMOD3*, *MAPK6*, and *TLN2*. These data imply that overexpression of *CYP19A1* in the inversion-positive cases are caused by cryptic usage of constitutively active promoters. Consistent with this, *in silico* analysis revealed the presence of promoter-compatible sequences around exon 1 of *CGN1*, *TMOD3*, and *MAPK6* in multiple cell types, although such sequences remain to be identified for noncoding exons of *TLN2* [4].

We recently studied 18 males from six families with AEXS (families A–F) and identified three types of heterozygous cryptic genomic rearrangements in the upstream region of the *CYP19A1* coding exons (Figure 2) [4]. In families A and B, we identified the same 79,156 bp tandem duplication encompassing seven of the 11 noncoding exons 1 of *CYP19A1*. Notably, this duplication includes exon I.4 that functions as a major promoter for extragonadal tissues such as fat and skin; therefore, *CYP19A1* overexpression in these families would be explained by increasing the number of this promoter. Indeed, RT-PCR analysis detected a splice variant consisting of exon I.4 at the 5′ side and exon I.8 at the 3′ side in lymphoblastoid cell lines and skin fibroblasts of the patients, indicating that the duplicated exon I.4 at the distal nonphysiological position actually functions as transcription start sites. In family C, we identified a 211,631 bp deletion affecting exons 2–43 of *DMXL2* and exons 5–10 of *GLDN*. This deletion appears to have caused *CYP19A1* overexpression because of cryptic usage of *DMXL2* exon 1 as an extra transcription start site for *CYP19A1*. Indeed, RT-PCR revealed the presence of chimeric mRNA clones consisting of *DMXL2* exon 1 and *CYP19A1* exon 2, supporting the notion that aberrant splicing has occurred between these two exons. Such *DMXL2/CYP19A1* chimeric mRNA accounted for 2–5% of *CYP19A1*-containing transcripts from skin fibroblasts. In families D–F, we identified

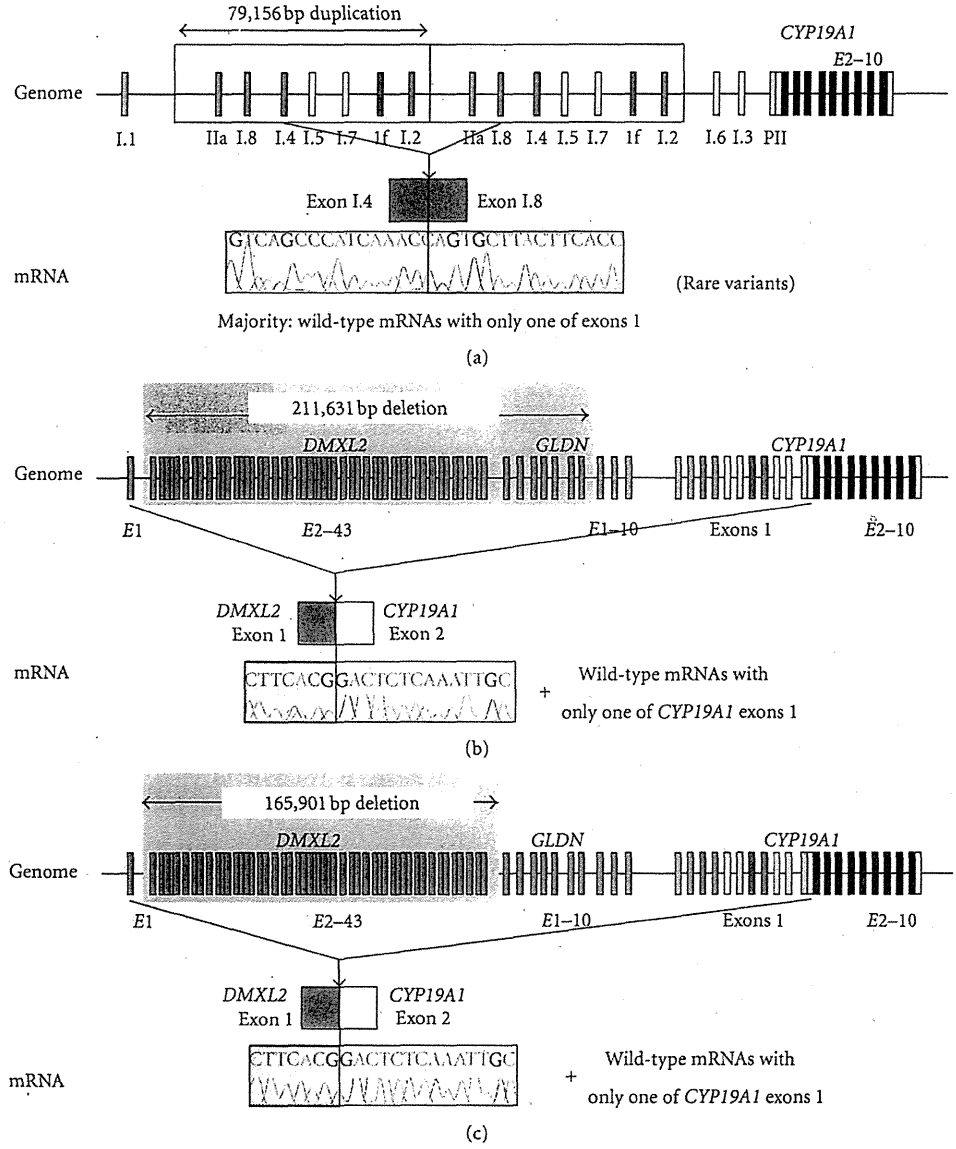

FIGURE 2: Schematic representation of duplications and deletions identified in patients with AEXS. (a) the tandem duplication of families A and B [4]. Genome: the duplication (yellow boxes) includes seven of the 11 noncoding exons 1 of *CYP19A1*. mRNA: the sequence of a rare transcript is shown. The 3′-end of exon I.4 is connected with the 5′-end of exon I.8. (b) The deletion of family C [4]. Genome: the deletion (a gray area) includes exons 2–43 of *DMXL2* and exons 5–10 of *GLDN*. mRNA: The sequence of a rare chimeric gene transcript is shown. *DMXL2* exon 1 consisting of a noncoding region and a coding region is spliced onto the common acceptor site of *CYP19A1* exon 2. (c) The deletion of families D–F [4]. Genome: the deletion (a gray area) includes exons 2–43 of *DMXL2*. mRNA: the sequence of a rare chimeric gene transcript is delineated. The mRNA structure is the same as that detected in family C.

an identical 165,901 bp deletion including exons 2–43 of *DMXL2*. RT-PCR identified the same chimeric mRNA as that detected in family C.

Collectively, three types of genomic rearrangements on 15q21 have been identified in AEXS to date, namely, inversion type (four subtypes), duplication type, and deletion type (two subtypes) (Figure 3(a)) [2–4]. In this regard, sequence analyses for the breakpoints have indicated that (1) inversion types are formed by a repeat sequence-mediated nonallelic intrachromosomal or interchromosomal recombination or by a replication-based mechanism of fork stalling and template switching (FoSTeS) that occurs in the absence of repeat sequences and is often associated with microhomology [16], (2) duplication type is generated by FoSTeS, and (3) deletions are produced by nonhomologous end joining that takes place between nonhomologous sequences and is frequently accompanied by an insertion of a short segment at the fusion point or by a nonallelic recombination [16].

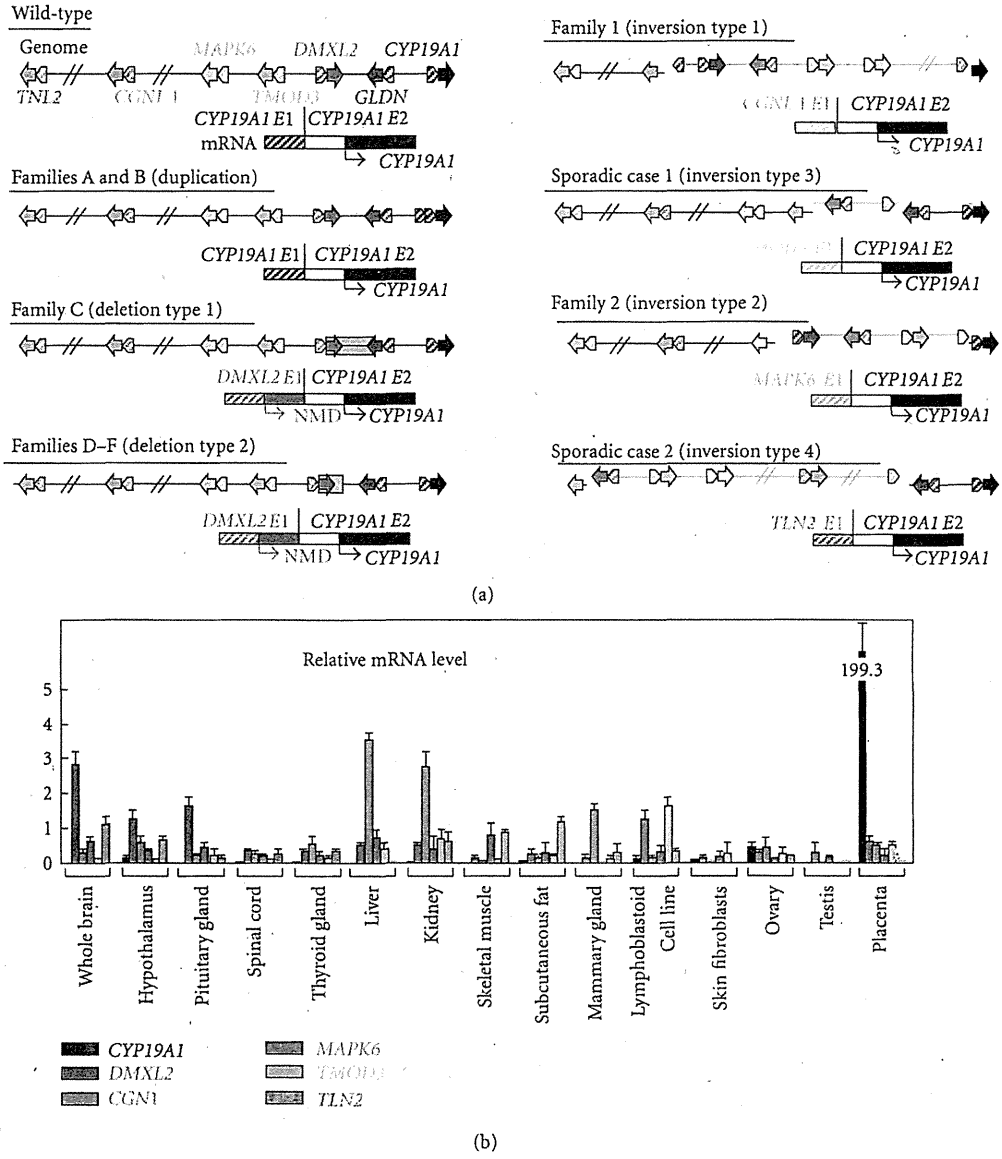

FIGURE 3: Structural and functional properties of the fused exons. (a) Schematic representation of the rearranged genome and mRNA structures. The white and the black boxes of *CYP19A1* exon 2 show untranslated region and coding region, respectively. For genome, the striped and the painted arrows indicate noncoding and coding exons, respectively (5′ → 3′). The inverted genomic regions are delineated in blue lines. For mRNA, colored striped boxes represent noncoding regions of each gene. The *DMXL2-CYP19A1* chimeric mRNA has two translation initiation codons and therefore is destined to produce not only *CYP19A1* protein but also a 47 amino acid protein which is predicted to undergo nonsense-mediated mRNA decay (NMD). The deletion and the inversion types are associated with heterozygous impairment of neighboring genes (deletion or disconnection between noncoding exon(s) and the following coding exons). The inversion subtype 1 is accompanied by inversion of eight of the 11 *CYP19A1* exons 1, and the inversion subtype 2 is associated with inversion of the placenta-specific *CYP19A1* exon I.1. (b) Expression patterns of *CYP19A1* and the five neighboring genes involved in the chimeric gene formation [4]. Relative mRNA levels against *TBP* in normal human tissues are shown.

Thus, it appears that genomic sequence around *CYP19A1* harbors particular motifs that are vulnerable to replication- and recombination-mediated errors. The results provide novel mechanisms of gain-of-function mutations leading to human diseases.

4. Clinical Features of AEXS

To date, a total of 23 male cases from 10 families have been reported to have molecularly confirmed AEXS (Table 1, Figure 3(a)) [2–4]. They exhibited pre- or peripubertal onset

Table 1: Summary of clinical studies in male patients with aromatase excess syndrome (modified from [4]).

(a)

Family			Family A			Family B		Family C				Family D			Family E	
Mutation types			Duplication			Duplication		Deletion				Deletion			Deletion	
The promoter involved in *CYP19A1* overexpression			*CYP19A1*			*CYP19A1*		*CYP19A1*				*DMXL2*			*DMXL2*	
Case		Case 1	Case 2		Case 3	Case 4		Case 5		Case 6	Case 7	Case 8		Case 9	Case 10	
Age at examination (year)		66	15		20	15		15		13	42	9		12	13	
<Phenotypic findings>																
Gynecomastia (tanner breast stage)		**2**	**2**		**2**	**3**		**4**		**4**	**4**	**3**		**4**	**4**	
Onset of gynecomastia (year)		**13**	**13**		**10**	**11**		**12**		**11**	**11**	**7**		**9**	**10**	
Mastectomy (year)		No	**Yes (15)**		No	**Yes (15)**		**Yes (15)**		**Yes (13)**	No	No		**Yes (12)**	**Yes (13)**	
Testis (ml)		N.E.	**12**		**12**	**12**		**12**		12	N.E.	3		12	20	
Pubic hair (tanner stage)		N.E.	2-3		4	5		4		3	N.E.	1		3	4	
Facial hair		Normal	Scarce		**Scarce**	Normal		Absent		Absent	N.E.	Absent		Absent	Absent	
Height (SDS)[a]		−1.2	−0.3		+0.4	+0.8		−2.0		−1.0	−1.6	**+2.7**		±0	+1.8	
Bone age (year)[b]		N.E.	N.E.		N.E.	16.0		16.0		13.5	N.E.	**13.0**		**15.0**	**17.0**	
Fertility (spermatogenesis)		Yes	?		(Yes)[h]	?		?		?	Yes	?		?	?	
<Endocrine findings>[c]		B	B	S	B S	B	S	B	S	B S	B	B	S	B S	B	S
<At Dx>	Stimulus															
LH (mIU/mL)	GnRH[e]	3.8	2.3	**14.3**	2.1 **17.0**	2.4	29.4	1.9	40.6	1.8	69.2	1.1	11.5	**0.6**	39.5	6.7	14.8
LH (mIU/mL)	GnRH (after priming)[f]		1.8	**9.5**	**1.3** **10.7**												
FSH (mIU/mL)	GnRH[e]	**1.7**	**3.1**	**5.3**	**<0.5** **1.2**	**0.9**	**2.4**	**1.4**	**4.2**	**2.0**	**7.8**	**3.2**	**6.6**	**0.6**	**2.9**	**0.7**	**1.0**
FSH (mIU/mL)	GnRH (after priming)[f]		**2.6**	**3.2**	**<0.5** **0.9**												
Prolactin (ng/ml)			4.3		5.3			8.2		9.1		11.3		18.8			
Δ^4A (ng/mL)		**0.5**			**1.1**	**1.2**					**0.6**			**0.7**		**2.4**	2.9
T (ng/mL)	hCG[g]	2.9	**1.6**		**2.2**	4.0		**2.6**	7.2	**1.4**	7.9	**0.6**	3.6	**2.4**		3.2	9.7
DHT (ng/mL)		0.4			0.2											0.4	1.2
Inhibin B (pg/mL)		**61.6**			**74.6**	**83.5**		**75.2**									
E_1 (pg/mL)		157			120	124					57			63		53	
E_2 (pg/mL)		29	15		22	59		56		38	24	19		25		58	
E_2/T ratio ($\times 10^3$)		10.0	9.4		10.0	14.8		21.5		27.1		31.7		10.4		18.1	

(b)

Family		Family F								Family G		Family H		Sporadic	
Mutation types		Deletion								Inversion		Inversion		Inversion	
The promoter involved in *CYP19A1* overexpression		*DMXL2*								*CGNL1*		*MAPK6*		*TMOD3*	*TLN2*
Case		Case 11	Case 12	Case 13	Case 14	Case 15	Case 16	Case 17	Case 18	Case 19	Case 20	Case 21[j]		Case 22	Case 23
Age at examination (year)		69	35	44	45	9	8	13	10	35	7	13		17	36
<Phenotypic findings>															
Gynecomastia (tanner breast stage)		**Yes**[i]	**Yes**[i]	**Yes**[i]	**Yes**[i]	**2**	**3**	**3**	**3**	**Yes**	**3**	**5**		N.E.	**Yes**
Onset of gynecomastia (year)		?	?	?	?	**8**	**8**	**11**	**10**	**5**	**5**	**8**		**7**	?
Mastectomy (year)		**Yes**[i]	**Yes**[i]	**Yes**[i]	**Yes**[i]	No	No	**Yes (?)**	**Yes (?)**	**Yes (16)**	No	**Yes (?)**		**Yes (?)**	**Yes (19)**
Testis (ml)		N.E.	N.E.	N.E.	N.E.	2	1.5	**2**	2	N.E.	N.E.	N.E.		Normal	N.E.
Pubic hair (tanner stage)		N.E.	N.E.	N.E.	N.E.	1	1	2	1	Normal	1	**2-3** (at 21.0)		N.E.	N.E.
Facial hair		N.E.	N.E.	N.E.	N.E.	Absent	Absent	Absent	Absent	**Absent**	Absent	N.E.		**Scarce**	N.E.
Height (SDS)[a]		N.E.	~ −1.5	~ −1.5	~ −1.5	+1.4	N.E.	**+2.0**	**+2.4**	**Short**	**>+2.5**	−1.6 (at 21.0)		**Short**	N.E.
Bone age (year)[b]		N.E.	N.E.	N.E.	N.E.	**12.5**	**13.0**	**15.0**	**14.5 (at 12.5)**	N.E.	**13.0 (at 5.5)**	**17.0**		N.E.	N.E.
Fertility (spermatogenesis)		Yes	Yes	Yes	Yes	?	?	?	?	Yes	?	?		?	?
<Endocrine findings>[c]		B	B	B	B	B	B	B S	B	B	B	B	S	B	
<At Dx>	Stimulus														
LH (mIU/mL)	GnRH[e]	**0.2**	3.5	1.7	3.0	0.2	<0.1	2.6 6.3	1.5	1.7	0.1	2.6	**10.0**	4.3	
LH (mIU/mL)	GnRH (after priming)[f]														
FSH (mIU/mL)	GnRH[e]	**1.4**	**2.3**	**0.8**	**0.8**	1.4	0.5	**0.8** 1.2	**1.2**	**1.5**	0.3	**<0.1**	**<0.1**	**2.7**	
FSH (mIU/mL)	GnRH (after priming)[f]														
Prolactin (ng/ml)															
Δ^4A (ng/mL)		1.4	**0.4**	1.7	**0.5**	0.3	<0.3	**0.9** 1.5	1.3	**0.8**	0.3	2.4	**0.9**		
T (ng/mL)	hCG[g]	**2.6**	**2.5**	**2.1**	**2.5**	<0.1	<0.1	**2.7** 9.2	**2.7**	3.2	<0.1	**1.2**	3.8	**2.3**	
DHT (ng/mL)												0.2	0.5		
Inhibin B (pg/mL)															
E_1 (pg/mL)		32	34	59	34	26	41	77	86	903	119	544		556	
E_2 (pg/mL)		10	19	24	31	11	7	25	40	223	15	178		392	
E_2/T ratio ($\times 10^3$)		3.8	7.6	11.4	12.4			9.3	14.8	69.6		148.3		170.4	

SDS: standard deviation score; Dx: diagnosis; Tx: therapy; LH: luteinizing hormone; FSH: follicle stimulating hormone; Δ^4A: androstenedione; T: testosterone; DHT: dihydrotestosterone; E_1: estrone; E_2: estradiol; GnRH: gonadotropin-releasing hormone; hCG: human chorionic gonadotropin; N.E.: not examined; B: basal; and S: stimulated.

Abnormal clinical findings are boldfaced.

Abnormally low hormone values are boldfaced, and abnormally high hormone values are underlined.

[a]Evaluated by age- and ethnicity-matched growth references; heights ≥+2.0 SD or below ≤ −2.0 SD were regarded as abnormal.

[b]Assessed by the Tanner-Whitehouse 2 method standardized for Japanese or by the Greulich-Pyle method for Caucasians; bone age was assessed as advanced when it was accelerated a year or more.

[c]Evaluated by age-matched male reference data, except for inhibin B and E_1 that have been compared with data from 19 adult males.

[d]Treated with aromatase inhibitors (anastrozole).

[e]GnRH 100 μg/m^2 (max. 100 μg) bolus i.v.; blood sampling at 0, 30, 60, 90, and 120 minutes.

[f]GnRH test after priming with GnRH 100 μg i.m. for 5 consecutive days.

[g]hCG 3000 IU/m^2 (max 5000 IU) i.m. for 3 consecutive days; blood sampling on days 1 and 4.

[h]Although Case 3 has not yet fathered a child, he has normal spermatogenesis with semen volume of 2.5 ml (reference value: >2 ml), sperm count of 105 × 10^6/ml (>20 × 10^6/ml), total sperm count of 262.5 × 10^6 (>40 × 10^6), motile cells of 70% (>50%), and normal morphological sperms 77% (>30%).

[i]These four patients allegedly had gynecomastia that required mastectomy (age unknown).

[j]The sister has macromastia, large uterus, and irregular menses; the parental phenotype has not been described.

The conversion factor to the SI unit: LH 1.0 (IU/L), FSH 1.0 (IU/L), E_1 3.699 (pmol/L), E_2 3.671 (pmol/L), Δ^4A 3.492 (nmol/L), and T 3.467 (nmol/L).

gynecomastia, small testes with fairly preserved masculinization, obvious or relative tall stature in childhood and grossly normal or apparent short stature in adulthood, and age-appropriate or variably advanced bone ages. Blood endocrine studies revealed markedly elevated E_1 values and E_2/T ratios in all cases examined and normal or variably elevated E_2 values. In addition, Δ^4-androstenedione, T, and dihydrotestosterone values were low or normal, and human chorionic gonadotropin (hCG) test indicated normal T responses. Notably, LH values were grossly normal at the baseline and variably responded to GnRH stimulation, whereas FSH values were low at the baseline and poorly responded to GnRH stimulation even after preceding GnRH priming, in all cases examined.

The severity of such clinical phenotypes is primarily dependent on the underlying mechanisms (Table 1). They are obviously mild in the duplication type, moderate in the deletion type, and severe in the inversion type, except for serum FSH values that remain suppressed irrespective of the underlying mechanisms. Likewise, gynecomastia has been reported to be ameliorated with 1 mg/day of aromatase inhibitor (anastrozole) in the duplication and the deletion types and with 2–4 mg/day of anastrozole in the inversion type [4].

5. Expression Pattern of *CYP19A1* and the Chimeric Genes as One Phenotypic Determinant

Phenotypic severity is much milder in the duplication type than in the deletion and the inversion types. This would be explained by the tissue expression pattern of *CYP19A1* and the chimeric genes. Indeed, RT-PCR analysis using normal human tissue samples revealed that *CYP19A1* is expressed only in a limited number of tissues such as placenta, ovary, skin, and fat, while the five genes involved in the formation of chimeric genes are widely expressed with some degree of variation (Figure 3(b)). Therefore, it is likely that the duplication types would simply increase *CYP19A1* transcription in native *CYP19A1*-expressing tissues, whereas the deletion and the inversion types lead to *CYP19A1* overexpression in a range of tissues, because expression patterns of chimeric genes are predicted to follow those of the original genes. Furthermore, it is also likely that the native *CYP19A1* promoter is subject to negative feedback by elevated estrogens [17], whereas such negative feedback effect by estrogen is weak or even absent for the chimeric genes in the deletion and the inversion types.

6. Structural Property of the Fused Exons as Another Phenotypic Determinant

Phenotypic severity is also milder in the deletion type than in the inversion types, despite a similar wide expression pattern of genes involved in the chimeric gene formation (Table 1, Figure 3(b)). In this context, it is noteworthy that a translation start codon and a following coding region are present on exon 1 of *DMXL2* of the deletion type but not on exons 1 of the chimeric genes of the inversion types (Figure 3(a)). Thus, it is likely that *DMXL2/CYP19A1* chimeric mRNAs transcribed by the *DMXL2* promoter preferentially recognize the natural start codon on *DMXL2* exon 1 and undergo nonsense-mediated mRNA decay and that rather exceptional chimeric mRNAs, which recognize the start codon on *CYP19A1* exon 2, are transcribed into CYP19A1 protein. By contrast, such a phenomenon would not be postulated for the inversion-mediated chimeric mRNAs. Consistent with this, it has been shown that the *DMXL2/CYP19A1* chimeric mRNA is present only in 2–5% of *CYP19A1*-containing transcripts from skin fibroblasts, whereas the *CGNL1/CYP19A1* chimeric mRNA and the *TMOD3/CYP19A1* chimeric mRNA account for 89–100% and 80% of transcripts from skin fibroblasts, respectively [2, 4].

In addition, the genomic structure caused by the rearrangements would affect efficiency of splicing between noncoding exon(s) of neighboring genes and *CYP19A1* exon 2. For example, in the inversion subtype 1, the physical distance between *CGNL1* exon 1 and *CYP19A1* exon 2 is short, and, while a splice competition may be possible between exon 1 of neighboring genes and original *CYP19A1* exons 1, eight of 11 *CYP19A1* exons 1 including exon I.4 have been disconnected from *CYP19A1* coding exons by inversion (Figure 3(a)). This may also enhance the splicing efficiency between *CGNL1* exon 1 and *CYP19A1* exon 2 and thereby lead to relatively severe overexpression of the *CGNL1-CYP19A1* chimeric gene, although this hypothesis would not be applicable for other chimeric genes.

7. Implication for the Hypothalamus-Pituitary-Gonadal Axis Function

It is notable that a similar degree of FSH-dominant hypogonadotropic hypogonadism is observed in the three types, although E_1 and E_2 values and E_2/T ratios are much higher in the inversion type than in the duplication and deletion types (Table 1). In particular, FSH was severely suppressed even after GnRH priming in the duplication type [4]. This implies that a relatively mild excess of circulatory estrogens can exert a strong negative feedback effect on FSH secretion primarily at the pituitary. This would be consistent with the results of animal studies that show strong inhibitory effect of E_2 on transcription of FSH beta-subunit gene in the pituitary cells and almost negligible effect on synthesis of LH beta-subunit and secretion of LH [18, 19]. In this regard, while T responses to hCG stimulation are normal in the duplication and the deletion types and somewhat low in the inversion type, this would be consistent with fairly preserved LH secretion in the three types and markedly increased estrogen values in the inversion type. In addition, whereas fertility and spermatogenesis are normally preserved in the three types, this would be explained by the FSH-dominant hypogonadotropic hypogonadism, because FSH plays only a minor role in male fertility (spermatogenesis) [20].

8. Conclusions

Current studies argue that AEXS is caused by overexpression of *CYP19A1* due to three different types of cryptic genomic rearrangements including duplications, deletions, and inversions. It seems that transcriptional activity and structural property of the fused promoter constitutes the underlying factor for the clinical variability in most features of AEXS except for FSH-dominant hypogonadotropic hypogonadism. Thus, AEXS represents a novel model for gain-of-function mutation leading to human genetic disorders.

References

[1] S. Bhasin, "Testicular disorders," in *Williams Textbook of Endocrinology*, H. M. Kronenberg, M. Melmed, K. S. Polonsky, and P. R. Larsen, Eds., pp. 645–699, Saunders, Philadelphia, Pa, USA, 11th edition, 2008.

[2] M. Shozu, S. Sebastian, K. Takayama et al., "Estrogen excess associated with novel gain-of-function mutations affecting the aromatase gene," *New England Journal of Medicine*, vol. 348, no. 19, pp. 1855–1865, 2003.

[3] M. Demura, R. M. Martin, M. Shozu et al., "Regional rearrangements in chromosome 15q21 cause formation of cryptic promoters for the CYP19 (aromatase) gene," *Human Molecular Genetics*, vol. 16, no. 21, pp. 2529–2541, 2007.

[4] M Fukami, M Shozu, S Soneda et al., "Aromatase excess syndrome: identification of cryptic duplications and deletions leading to gain of function of CYP19A1 and assessment of phenotypic determinants," *The Journal of Clinical Endocrinology & Metabolism*, vol. 96, no. 6, pp. E1035–E1043, 2011.

[5] G. Binder, D. I. Iliev, A. Dufke et al., "Dominant transmission of prepubertal gynecomastia due to serum estrone excess: Hormonal, biochemical, and genetic analysis in a large kindred," *Journal of Clinical Endocrinology and Metabolism*, vol. 90, no. 1, pp. 484–492, 2005.

[6] R. M. Martin, C. J. Lin, M. Y. Nishi et al., "Familial hyperestrogenism in both sexes: clinical, hormonal, and molecular studies of two siblings," *Journal of Clinical Endocrinology and Metabolism*, vol. 88, no. 7, pp. 3027–3034, 2003.

[7] A. Tilpakov, N. Kalintchenko, T. Semitcheva et al., "A potential rearrangement between CYP19 and TRPM7 genes on chromosome 15q21.2 as a cause of aromatase excess syndrome," *The Journal of Clinical Endocrinology & Metabolism*, vol. 90, pp. 4184–4190, 2005.

[8] C. A. Stratakis, A. Vottero, A. Brodie et al., "The aromatase excess syndrome is associated with feminization of both sexes and autosomal dominant transmission of aberrant p450 aromatase gene transcription," *Journal of Clinical Endocrinology and Metabolism*, vol. 83, no. 4, pp. 1348–1357, 1998.

[9] S. Sebastian and S. E. Bulun, "Genetics of endocrine disease: a highly complex organization of the regulatory region of the human CYP19 (Aromatase) gene revealed by the human genome project," *Journal of Clinical Endocrinology and Metabolism*, vol. 86, no. 10, pp. 4600–4602, 2001.

[10] S. E. Bulun, K. Takayama, T. Suzuki, H. Sasano, B. Yilmaz, and S. Sebastian, "Organization of the human aromatase P450 (CYP19) gene," *Seminars in Reproductive Medicine*, vol. 22, no. 1, pp. 5–9, 2004.

[11] M. Demura, S. Reierstad, J. E. Innes, and S. E. Bulun, "Novel promoter I.8 and promoter usage in the CYP19 (aromatase) gene," *Reproductive Sciences*, vol. 15, no. 10, pp. 1044–1053, 2008.

[12] N. Harada, T. Utsumi, and Y. Takagi, "Tissue-specific expression of the human aromatase cytochrome P-450 gene by alternative use of multiple exons 1 and promoters, and switching of tissue-specific exons 1 in carcinogenesis," *Proceedings of the National Academy of Sciences of the United States of America*, vol. 90, no. 23, pp. 11312–11316, 1993.

[13] E. R. Simpson, "Aromatase: biologic relevance of tissue-specific expression," *Seminars in Reproductive Medicine*, vol. 22, no. 1, pp. 11–23, 2004.

[14] E. E. Wallach and C. R. Garcia, "Familial gynecomastia without hypogonadism: a report of three cases in one family," *The Journal of Clinical Endocrinology and Metabolism*, vol. 22, pp. 1201–1206, 1962.

[15] G. D. Berkovitz, A. Guerami, T. R. Brown, P. C. MacDonald, and C. J. Migeon, "Familial gynecomastia with increased extraglandular aromatization of plasma carbon19-steroids," *The Journal of Clinical Investigation*, vol. 75, no. 6, pp. 1763–1769, 1985.

[16] W. Gu, F. Zhang, and J. R. Lupski, "Mechanisms for human genomic rearrangements," *Pathogenetics*, vol. 1, article 4, 2008.

[17] M. B. Yilmaz, A. Wolfe, Y. H. Cheng, C. Glidewell-Kenney, J. L. Jameson, and S. E. Bulun, "Aromatase promoter I.f is regulated by estrogen receptor alpha (ESR1) in mouse hypothalamic neuronal cell lines," *Biology of Reproduction*, vol. 81, no. 5, pp. 956–965, 2009.

[18] J. E. Mercer, D. J. Phillips, and I. J. Clarke, "Short-term regulation of gonadotropin subunit mRNA levels by estrogen: studies in the hypothalamo-pituitary intact and hypothalamo-pituitary disconnected ewe," *Journal of Neuroendocrinology*, vol. 5, no. 5, pp. 591–596, 1993.

[19] D. C. Alexander and W. L. Miller, "Regulation of ovine follicle-stimulating hormone β-chain mRNA by 17β-estradiol in vivo and in vitro," *Journal of Biological Chemistry*, vol. 257, no. 5, pp. 2282–2286, 1982.

[20] T. R. Kumar, Y. Wang, N. Lu, and M. M. Matzuk, "Follicle stimulating hormone is required for ovarian follicle maturation but not male fertility," *Nature Genetics*, vol. 15, no. 2, pp. 201–204, 1997.

NOTE

Advance Publication
doi: 10.1507/endocrj.EJ12-0257

Neuromuscular symptoms in a patient with familial pseudohypoparathyroidism type Ib diagnosed by methylation-specific multiplex ligation-dependent probe amplification

Keisuke Nagasaki[1), 2)]*, Shuichi Tsuchiya[3)]*, Akihiko Saitoh[2)], Tsutomu Ogata[1), 4)] and Maki Fukami[1)]

[1)] *Department of Molecular Endocrinology, National Research Institute for Child Health and Development, Tokyo 157-8535, Japan*
[2)] *Division of Pediatrics, Department of Homeostatic Regulation and Development, Niigata University Graduate School of Medical and Dental Sciences, Niigata 951-8510, Japan*
[3)] *Department of Pediatrics, Ojiya general Hospital, Niigata 947-8641, Japan*
[4)] *Department of Pediatrics, Hamamatsu University School of Medicine, Hamamatsu 431-3192, Japan*

Abstract. Pseudohypoparathyroidism type Ib (PHP-Ib) is a rare genetic disorder characterized by hypocalcemia and hyperphosphatemia due to imprinting defects in the maternally derived *GNAS* allele. Patients with PHP-Ib are usually identified by tetany, convulsions, and/or muscle cramps, whereas a substantial fraction of patients remain asymptomatic and are identified by familial studies. Although previous studies on patients with primary hypoparathyroidism have indicated that hypocalcemia can be associated with various neuromuscular abnormalities, such clinical features have been rarely described in patients with PHP-Ib. Here, we report a 12-year-old male patient with familial PHP-Ib and unique neuromuscular symptoms. The patient presented with general fatigue, steppage gait, and myalgia. Physical examinations revealed muscular weakness and atrophies in the lower legs, a shortening of the bilateral Achilles' tendons and absence of deep tendon reflexes. Laboratory tests showed hypocalcemia, hyperphosphatemia, elevated serum intact PTH level, and impaired responses of urinary phosphate and cyclic AMP in an Ellsworth-Howard test, in addition to an elevated serum creatine kinase level. Clinical features of the patient were significantly improved after 1 month of treatment with alfacalcidol and calcium. Methylation-specific multiplex ligation-dependent probe amplification (MS-MLPA) and subsequent PCR analyses identified a methylation defect at exon A/B of *GNAS* and a microdeletion involving exons 4-6 of the *GNAS* neighboring gene *STX16* in the patient and in his asymptomatic brother. The results suggest that various neuromuscular features probably associated with hypocalcemia can be the first symptoms of PHP-Ib, and that MS-MLPA serves as a powerful tool for screening of GNAS abnormalities in patients with atypical manifestations.

Key words: PHP-Ib, Neuromuscular symptoms, Hypocalcemia, *STX16*, MS-MLPA

PSEUDOHYPOPARATHYROIDISM (PHP; MIM 103580) is a genetically heterogeneous condition characterized by hypocalcemia and hyperphosphatemia resulting from end-organ resistance to PTH [1]. PHP is classified into 2 subtypes, PHP-Ia and -Ib, according to the molecular causes and clinical features of the patients [1]. PHP-Ia results from loss-of-function mutations in the maternally derived *GNAS* gene that encodes the stimulatory G protein α-subunit [1]. Patients with PHP-Ia manifest multiple hormone resistance and characteristic physical stigmata such as short stature, obesity, round face, brachydactyly, subcutaneous ossification, and mild to moderate mental retardation, which are collectively referred to as Albright's hereditary osteodystrophy (AHO) [1, 2].

PHP-Ib is caused by imprinting defects of the maternally derived *GNAS* allele; patients with this condi-

Submitted Jul. 17, 2012; Accepted Oct. 14, 2012 as EJ12-0257
Released online in J-STAGE as advance publication Oct. 25, 2012
Correspondence to: Keisuke Nagasaki, Division of Pediatrics, Department of Homeostatic Regulation and Development, Niigata University Graduate School of Medical and Dental Sciences, Niigata, 951-8510, Japan. E-mail: nagasaki@med.niigata-u.ac.jp
Maki Fukami, Department of Molecular Endocrinology, National Research Institute for Child Health and Development, Tokyo 157-8535, Japan. E-mail: mfukami@nch.go.jp
* K.N. and S.T. contributed equally to this work.

tion show hypomethylation at one or more of the 4 differentially methylated regions (DMRs) of *GNAS* [3-7]. Genetic causes of PHP-Ib include cryptic deletions within the genes neighboring *GNAS*, *STX16* and *NESP55*, and epimutation of *GNAS* DMRs [4, 5]. Patients with PHP-Ib manifest PTH resistance without AHO [1]. These patients are usually identified by hypocalcemia-associated neuromuscular irritability, such as tetany, generalized convulsions, and/or muscle cramps, although a substantial fraction of the patients remain asymptomatic and are identified only by familial studies [6, 7].

Previous studies of patients with primary hypoparathyroidism have shown that hypocalcemia can be associated with various types of neuromuscular symptoms [8, 9]. However, such clinical features have been rarely described in patients with PHP-Ib [10]. Here, we report a Japanese patient with familial PHP-Ib due to an intragenic deletion of *STX16*, who presented with unique neuromuscular symptoms.

Methods

Case report

This male patient was born as the third child to non-consanguineous Japanese parents at 39 weeks of gestation, after an uncomplicated pregnancy and delivery. His birth weight was 3482 g (+1.1 SD) and length 50 cm (+0.7 SD). Neonatal screening tests were normal. His postnatal growth and development were uneventful.

From the age of 6 years, he had general fatigue. At 12 years of age, he was seen by a local doctor because of general fatigue, gait disturbance, and myalgia in the lower legs. He was suspected to have congenital myopathy, and was referred to our clinic for further investigation. His height and weight at the time of examination were 161.4 cm (+1.1 SD) and 42.4 kg (-0.2 SD), respectively. Physical examinations revealed muscular atrophies with weakness in the lower legs, a shortening of the bilateral Achilles' tendons and absence of deep tendon reflexes. He showed a high stepping gait with markedly reduced strength of dorsiflexors of the ankles. Sense of touch and temperature was normal. The Chvostek's sign was positive, while the Trousseau's sign was negative. He had neither AHO stigmata nor episodes of tetany or convulsions. Laboratory examinations revealed hypocalcemia, hyperphosphatemia, and an elevated serum intact PTH level, together with decreased urinary calcium excretions (Table 1). Serum creatine kinase (CK) level was markedly elevated. An Ellsworth-Howard test showed impaired responses of both urinary phosphaturic and cyclic AMP levels (Table 1). The TSH level was slightly elevated, while free T4 and gonadotropin levels were within the normal range. The serum 1,25-dihydroxy vitamin D (1,25(OH)2D) level was mildly elevated. Head computerized tomography (CT) delineated symmetric calcifications of the basal ganglia and thalami, and subcortical calcification of the right middle frontal gyrus. Dual-energy X-ray absorptiometry (DEXA) revealed decreased bone mineral density at the lumbar spine (L2-L4) (0.640 g/cm^2, -2.9 SD). Based on these data, we diagnosed him as having PHP-Ib with neuromuscular symptoms. After 1 month of treatment with alfacalcidol (1.5 μg/day) and calcium lactate (3.0 g/day), his general fatigue, gait disturbance, and myalgia were markedly improved.

The 15-year-old brother of the patient manifested no clinically discernible phenotype; the brother had no gait disturbance or muscle weakness. Furthermore, physical examinations revealed neither muscular atrophy nor neurologic abnormalities. However, laboratory examinations detected an elevated serum intact PTH level, although serum calcium level was within the normal range (Table 1). Thus, the brother was also suspected as having PHP-Ib. The brother manifested mildly elevated serum 1,25(OH)2D level.

The 50-year-old father and 17-year-old sister were clinically normal. The mother, deceased at 49 years of age of an unknown cause, allegedly had no clinical symptoms indicative of PHP. Endocrine studies revealed no abnormalities in the father, sister, or mother (Table 1).

Molecular analyses

This study was approved by the Institutional Review Board Committee at the National Center for Child Health. After obtaining written informed consent, we extracted genomic DNA from leukocytes of the patient and his brother and father.

We examined mutations in the coding region of *GNAS* by direct sequencing, and copy number alternations and methylation defects in the *GNAS*-flanking region by methylation-specific multiplex ligation-dependent probe amplification (MS-MLPA), using a commercially available probe mix (SALSA MLPA kit, ME031-A1) (MRC-Holland, Amsterdam, The Netherlands). To confirm the results of MS-MLPA, we performed PCR analyses using forward and reverse

Table 1 Laboratory findings of the patient and his family members

	Patient	Brother	Father	Mother	Sister	Reference range
Age at the examinations (years)	12	15	50	43	17	
Height (cm) (SDS)	161.4 (+1.1)	171 (+0.1)	N.A.	N.A.	N.A.	
Weight (kg) (SDS)	42.4 (-0.2)	53 (-0.9)	N.A.	N.A.	N.A.	
<Blood>						
Intact PTH (pg/mL)	**430**	**254**	26	44	26	10-65
Calcium (mg/dL)	**6.4**	8.9	9.3	8.7	9.2	8.5-10.2
Phosphate (mg/dL)	**9.1**	**5.2**	2.9	3.8	3.4	2.4-4.3
Magnesium (mg/dL)	1.8	2.0	N.A.	N.A.	N.A.	1.8-2.5
Na (mEq/l)	142	140	N.A.	N.A.	N.A.	135-147
K (mEq/l)	4.1	4.0	N.A.	N.A.	N.A.	3.6-5.0
Creatinine (mg/dL)	0.6	0.7	N.A.	N.A.	N.A.	0.4-1.1
Alb (g/dL)	4.9	4.5	N.A.	N.A.	N.A.	3.9-5.1
CK (IU/L)	**741**	136	N.A.	N.A.	N.A.	0-170
ALP (IU/L)	**1809** (388-1190)[a]	648 (225-680)[a]	N.A.	N.A.	N.A.	
1,25(OH)2D (pg/mL)	**69**	**79**	N.A.	N.A.	N.A.	20-60
TSH (mU/L)	**5.6**	4.1	N.A.	N.A.	N.A.	0.5-5.0
Free T4 (ng/dL)	1.0	1.0	N.A.	N.A.	N.A.	0.9-1.6
<Urine>						
Calcium/Creatinine ratio	**0.004**	**0.008**	N.A.	N.A.	N.A.	0.08-0.20
%TRP	**99.6**	**99.6**	N.A.	N.A.	N.A.	89.6-93.6
<Ellsworth-Howard test>						
Urinary phosphate (mg/2 hrs)[b]	**8.33**	N.A.	N.A.	N.A.	N.A.	≥30
Urinary cAMP (μmol/hr)[c]	**0.029**	N.A.	N.A.	N.A.	N.A.	≥1.0

The conversion factors to the international system of units (SI unit) are as follows: intact PTH 1.0 (ng/liter), serum calcium 0.25 (mmol/liter), serum phosphate 0.3229 (mmol/liter) serum magensium 0.411 (mmol/liter), serum sodium 1.0 (mmol/liter), serum potassium 1.0 (mmol/liter), serum creatine 88.4 (μmol/liter), serum albumin 10 (g/liter), serum 1,25(OH)2D 2.6 (pmol/liter), serum Free T4 12.9 (pmol/liter). Hormone values have been evaluated by the age- and sex-matched Japanese reference data; abnormal data are in bold.

[a] The values in parentheses indicate the age-and sex-matched reference laboratory data.

[b] Urinary phosphate denotes the increment of 2 hours urinary excretion of phosphate after injection of human PTH (100 unit).

[c] Urinary cAMP denote the increment of 1 hour urinary cAMP excretion after injection of human PTH (100 unit).

N.A., not analysed; CK, creatine kinase; 1,25(OH)2D, 1,25-dihydroxy vitamin D; %TRP, % tubular reabsorption of phosphate

primers that hybridize to introns 3 and 6 of *STX16*, respectively [4].

Results

Direct sequence analysis for the patient identified no mutation in the coding region of *GNAS*. However, MS-MLPA revealed decreased peak heights of probes that correspond to exons 5 and 6 of *STX16*, indicating a heterozygous deletion within *STX16*. In addition, MS-MLPA indicated hypomethylation at *GNAS* exon A/B and a normal methylation pattern of the other 3 *GNAS* DMRs (Fig. 1A, B). Subsequent PCR analyses showed the presence of a heterozygous 3 kb deletion involving exons 4-6 of *STX16* (STX16Δexons 4-6) (Fig. 1C). The microdeletion and methylation defect were also observed in the brother, but not in the father. DNA samples of the mother and the sister were not available for genetic analyses.

Discussion

We report here a Japanese patient with PHP-Ib, who was identified by general fatigue, gait disturbance, and myalgia in the lower legs. He showed muscular atrophies in the lower legs, a shortening of the bilateral Achilles' tendons, absence of deep tendon reflexes, and an elevated serum CK value. Such clinical features are indicative of neuromuscular symptoms, although a detailed neurological workup was not performed for

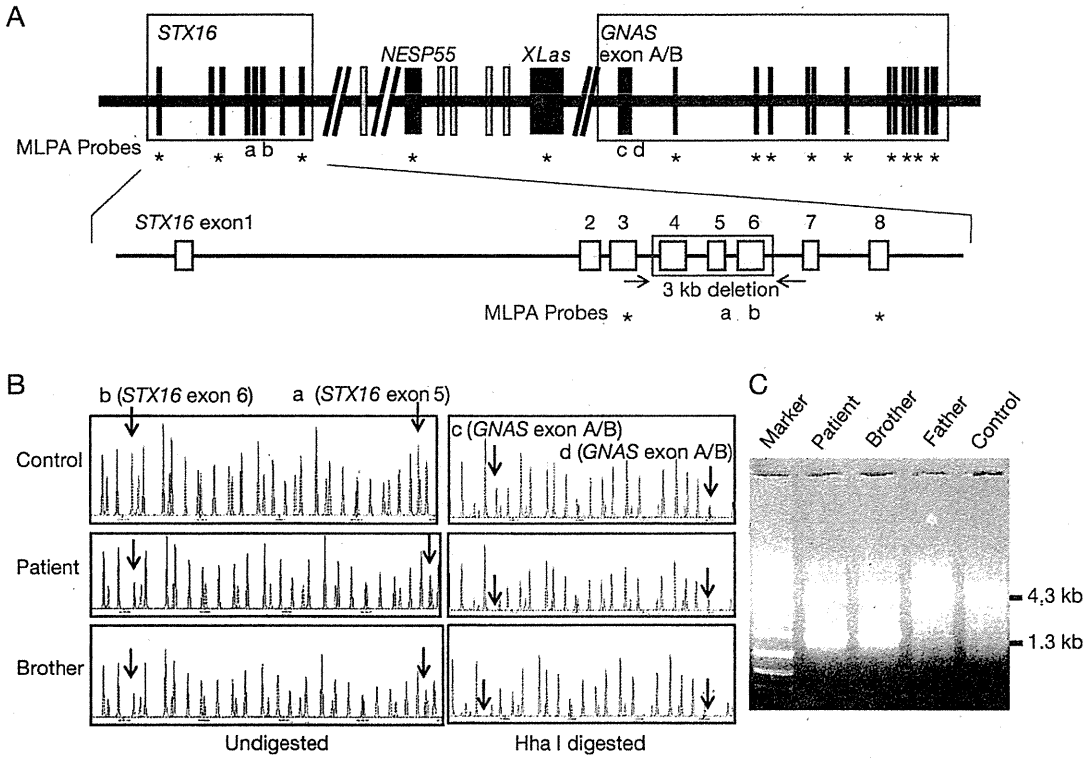

Fig. 1 Molecular analysis of the patient and his family members.
A, Schematic representation of the genomic region around *GNAS*. Upper panel: The loci examined by methylation-specific multiplex ligation-dependent probe amplification (MS-MLPA) are indicated by letters (a-d) and asterisks. Lower panel: Microdeletion identified in the patient and his brother. Horizontal arrows indicate the binding sites of the primers used for PCR analysis.
B. Representative results of MS-MLPA. Left panel: Decreased peak heights with probes a and b in the patient and his brother indicate heterozygous deletion involving exons 5 and 6 of *STX16*. Right panel: Absence of peaks with probes c and d indicate hypomethylation of *GNAS* exon A/B.
C, PCR analysis using a primer pair flanking the deletion. Both the 4.3 kb (wild-type) and 1.3 kb (STX16Δexons4-6) products were amplified from the patient and his brother, while only the 4.3 kb product was obtained from the father and the control individual.

this patient. In this regard, it is noteworthy that peripheral neuropathy and metabolic myopathy have been reported in patients with primary hypoparathyroidism [8, 9], whereas such symptoms have not been described in patients with PHP, except for mildly elevated blood CK and lactate dehydrogenase (LDH) levels in a single case of PHP-Ia [10]. Moreover, *in vitro* experiments showed that calcium concentration affects excitability at neuromuscular junctions [11]. Thus, the neuromuscular symptoms of our patient are likely to be associated with hypocalcemia. A significant improvement in the clinical features of the patient after 1 month of treatment with alfacalcidol and calcium supports this hypothesis. However, we cannot exclude the possibility that other factors such as vitamin D deficiency may also have played a role in the development of these features. Indeed, slightly elevated serum levels of ALP and 1,25(OH)2D in the patient are consistent with mild vitamin D deficiency [12]. On the other hand, since serum 1,25(OH)2D levels were similarly elevated in the patient and his asymptomatic brother, phenotypic variation in this family can not be explained by vitamin D deficiency. These results indicate that neuromuscular features probably associated with hypocalcemia can be the first symptoms of PHP-Ib. Nevertheless, this notion is based on observations of a single case, and

requires further investigations.

Both the patient and his brother carried a heterozygous STX16Δexons4-6. Although DNA samples of the mother were not available for genetic analyses, the absence of the deletion in the father indicated the maternal inheritance of the deletion. It has been shown that maternally inherited STX16Δexons4-6 (STX16Δexons4-6mat) is associated with hypomethylation at *GNAS* exon A/B, whereas *GNAS* epimutations are usually accompanied by methylation defects not only at exon A/B but also at other *GNAS* DMRs [3, 7]. These results suggest that the 3 kb region around exon 4-6 of *STX16* contains a cis-acting element that regulates methylation status at *GNAS* exon A/B. Consistent with this, our patient and his brother had methylation defects exclusively at exon A/B. Further studies are necessary to clarify the mechanism by which a DNA element >200 kb from *GNAS* controls the methylation status at exon A/B.

Clinical severities of patients with PHP-Ib are known to be variable [6, 7]. Notably, Linglart *et al.* have shown that STX16Δexons4-6mat is often associated with a mild phenotype. They found that about 40% of patients carrying this microdeletion remained asymptomatic, and more than 50% of asymptomatic individuals had normocalcemia at the time of diagnosis [7]. Consistent with this, our patient and his brother lacked typical PHP-Ib features such as tetany, generalized convulsions, or muscle cramps. Furthermore, the brother had normocalcemia. These results suggest that physical examinations and measurement of serum calcium levels are not sufficient to identify patients with PHP-Ib, and that genetic analyses or detailed endocrine evaluations, such as measurement of intact PTH levels and an Ellsworth-Howard test, are necessary for patients with atypical manifestations. In this context, although STX16Δexons4-6mat is the most frequent genetic cause of familial PHP-Ib [7], microdeletions affecting *NESP55* as well as epimutations of *GNAS* DMR also account for etiology of PHP-Ib [5, 7]. Since MS-MLPA is capable of detecting both copy number abnormalities and methylation defects in the *GNAS*-flanking region in a single assay, this method should be particularly useful for the molecular diagnosis of PHP-Ib.

In summary, the present study provides that various neuromuscular features probably associated with hypocalcemia can be the first symptoms of PHP-Ib, and suggests that MS-MLPA serves as a powerful tool for screening of *GNAS* abnormalities in patients with atypical manifestations.

Acknowledgments

We thank Dr. K. Kanno (Ojiya General Hospital) for providing us the blood samples of the family. We are also grateful to Ms. T. Tanji and E. Suzuki (National Research Institute for Child Health and Development) for their technical assistance, and Dr. J. Tohyama (Department of Pediatrics, Epilepsy Center, Nishi-Niigata Chuo National Hospital) for his fruitful discussion.

References

1. Levine MA (2000) Clinical spectrum and pathogenesis of pseudohypoparathyroidism. *Rev Endocr Metab Disord* 1: 265-274.
2. Weinstein LS, Yu S, Warner DR, Liu J (2001) Endocrine manifestations of stimulatory G protein alpha-subunit mutations and the role of genomic imprinting. *Endocr Rev* 22: 675-705.
3. Liu J, Litman D, Rosenberg MJ, Yu S, Biesecker LG, et al. (2000) A GNAS1 imprinting defect in pseudohypoparathyroidism type IB. *J Clin Invest* 106: 1167-1174.
4. Bastepe M, Frohlich LF, Hendy GN, Indridason OS, Josse RG, et al. (2003) Autosomal dominant pseudohypoparathyroidism type Ib is associated with a heterozygous microdeletion that likely disrupts a putative imprinting control element of GNAS. *J Clin Invest* 112: 1255-1263.
5. Bastepe M, Frohlich LF, Linglart A, Abu-Zahra HS, Tojo K, et al. (2005) Deletion of the NESP55 differentially methylated region causes loss of maternal GNAS imprints and pseudohypoparathyroidism type Ib. *Nat Genet* 37: 25-27.
6. Kinoshita K, Minagawa M, Takatani T, Takatani R, Ohashi M, et al. (2011) Establishment of diagnosis by bisulfite-treated methylation-specific PCR method and analysis of clinical characteristics of pseudohypoparathyroidism type 1b. *Endocr J* 58: 879-887.
7. Linglart A, Gensure RC, Olney RC, Juppner H, Bastepe M (2005) A novel STX16 deletion in autosomal dominant pseudohypoparathyroidism type Ib redefines the

boundaries of a cis-acting imprinting control element of GNAS. *Am J Hum Genet* 76: 804-814.
8. Kruse K, Scheunemann W, Baier W, Schaub J (1982) Hypocalcemic myopathy in idiopathic hypoparathyroidism. *Eur J Pediatr* 138: 280-282.
9. Goswami R, Bhatia M, Goyal R, Kochupillai N (2002) Reversible peripheral neuropathy in idiopathic hypoparathyroidism. *Acta Neurol Scand* 105: 128-131.
10. Piechowiak H, Grobner W, Kremer H, Pongratz D, Schaub J (1981) Pseudohypoparathyroidism and hypocalcemic "myopathy". A case report. *Klin Wochenschr* 59: 1195-1199.
11. Elmqvist D, Feldman DS (1965) Calcium dependence of spontaneous acetylcholine release at mammalian motor nerve terminals. *J Physiol* 181: 487-497.
12. Bringhurst FR, Demay MB, Kronenberg HM (2011) Hormones and disorders of mineral metabolism. In: Melmed S, Polonsky KS, Larson PR, Kronenberg HM (ed). Williams Textbook of endocrinology (12th). Saunders, Philadelphia: 1237-1304.

EUROPEAN JOURNAL OF Haematology

European Journal of Haematology 90 (164–168)

CASE REPORT

A novel Wiskott–Aldrich syndrome protein mutation in an infant with thrombotic thrombocytopenic purpura

Yukako Kawasaki[1], Hidemi Toyoda[1], Shoichiro Otsuki[1], Tadashi Iwasa[1], Shotaro Iwamoto[1], Eiichi Azuma[1], Naomi Itoh-Habe[2], Hideo Wada[2], Yoshihiro Fujimura[3], Tomohiro Morio[4], Kohsuke Imai[5], Noriko Mitsuiki[4,6], Osamu Ohara[6], Yoshihiro Komada[1]

[1]Department of Pediatrics, Mie University, Tsu, Mie, Japan; [2]Department of Molecular Laboratory Medicine, Mie University, Tsu, Mie, Japan; [3]Department of Blood Transfusion Medicine, Nara Medical University, Kashihara, Nara, Japan; [4]Department of Pediatrics, Tokyo Medical and Dental University, Tokyo, Japan; [5]Department of Pediatrics, National Defense Medical College, Tokorozawa, Saitama, Japan; [6]Department of Human Genome Research, Kazusa DNA Research Institute, Kisarazu, Chiba, Japan

Abstract

Thrombotic thrombocytopenic purpura (TTP) has not yet been reported to be associated with mutations in the Wiskott–Aldrich syndrome (WAS) gene. WAS is an X-linked recessive disorder characterized by thrombocytopenia, small platelet size, eczema, recurrent infections, and increased risk of autoimmune disorders and malignancies. A broad spectrum of mutations in the WAS protein (WASP) gene have been identified as causing the disease. In this study, we report on a 2-month-old Japanese boy who presented with cytomegalovirus (CMV) infection and TTP. The activity of von Willebrand factor cleaving metalloproteinase, ADAMTS13 was low and the antibody against ADAMTS13 was positive (3.6 Bethesda U/mL). Although TTP was improved by plasma exchange and steroid pulse therapy, thrombocytopenia persisted and regular transfusions of irradiated platelets were needed. Tiny platelets were found on a peripheral blood smear. CMV genome was positive in peripheral blood by polymerase chain reaction and the CMV viremia continued to persist despite intravenous gancyclovir therapy. Through direct sequencing of genomic DNA of the WASP gene in the patient, we identified a novel mutation of WASP gene: the seventh nucleotide in exon 11 (G) had been deleted (1345delG). This mutation causes a frameshift and a stop codon at amino acid 470. Western blotting demonstrated a truncated WAS protein. To our knowledge, this is the first report describing TTP in WAS patients with novel mutation in the WASP gene.

Key words Wiskott-Aldrich syndrome; thrombotic thrombocytopenic purpura; autoimmunity

Correspondence Hidemi Toyoda, MD, PhD, Department of pediatrics, Mie University School of Medicine, 2-174 Edobashi Tsu Mie 514-8507, Japan. Tel: +81 59 232 1111; Fax: +81 59 232 1111; e-mail: htoyoda@clin.medic.mie-u.ac.jp

Accepted for publication 6 December 2012

doi:10.1111/ejh.12057

Wiskott–Aldrich syndrome (WAS) is a rare X-linked disorder with variable clinical phenotypes that correlate with the type of mutations in the WAS protein (WASP) gene (1). The WASP gene is composed of 12 exons containing 1823 base pairs and encodes a 502-amino acid protein that appears to be of central importance for the function of hematopoietic stem cells (2). Mutations of WASP gene are located throughout the gene, although some hot spots have been identified (3). The type of mutation strongly influences the clinical severity of WAS (3). Mutations that abolish WASP expression are mainly associated with a severe clinical phenotype (full blown WAS) and a life expectancy below 20 yr of age (4). Mutations, on the other hand, result in residual expression of a full-length point-mutated WASP, are often associated with X-linked thrombocytopenia (XLT) (5), corresponding to a longer life expectancy (6). A scoring system based on clinical symptoms has been developed to differentiate these distinct clinical phenotypes caused by WASP gene mutations (2, 3, 7). Autoimmune complications are frequently observed in WAS and patients who develop autoimmune diseases are assigned to a high-risk group with poor prognosis (1). The incidence of autoimmunity in WAS is high in the US and European populations (40–72%), whereas a lower incidence was reported in Japan (22%)

(1, 6). The most common autoimmune manifestation in WAS is hemolytic anemia (36%), followed by vasculitis (including cerebral vasculitis; 29%), arthritis (29%), neutropenia (25%), inflammatory bowel disease (9%), and IgA nephropathy (3%) (8). Henoch–Schönlein purpura, dermatomyositis, recurrent angioedema, and uveitis have also been reported in some patients (6, 9). Moreover, in some cases, multiple autoimmune manifestations are observed.

Autoimmune hematological diseases are characterized by the production of antibodies against blood proteins and cells, and comprise immune thrombocytopenia, autoimmune hemolytic anemia, acquired hemophilia, and thrombotic thrombocytopenic purpura (TTP). TTP is a rare but severe disease characterized by mechanical hemolytic anemia and consumptive thrombocytopenia leading to disseminated microvascular thrombosis that causes signs and symptoms of organ ischemia and functional damage. von Willebrand factor (vWF) is synthesised in endothelial cells and assembled in larger multimers that are present in normal plasma. The larger multimers, called unusually large vWF (ULvWF), are rapidly degraded in the circulation into the normal size range vWF multimers by a specific vWF-cleaving protease, ADAMTS13 (a disintegrin-like and metalloprotease with thrombospondin type 1 motif 13) (10). ADAMTS13 deficiency leads sequentially to the accumulation of ULvWF multimers, platelet aggregation and platelet clumping, which is characteristic of the disease. ULvWF multimer accumulation in TTP is associated with absent or markedly diminished ADAMTS13 activity due to an inherited or acquired deficiency (11). An inhibitory autoantibody to the ADAMTS13 metalloproteinase has been found in patients with acquired TTP (11).

Here, we report a male infant who presented with cytomegalovirus (CMV) infection and acquired TTP which led to the diagnosis of WAS. A novel mutation, one nucleotide deletion at position 1345 (1345delG) in exon 11 was identified. To our knowledge, this is the first report regarding WAS with TTP as an autoimmune disease.

Materials and methods

Flow cytometric analysis of WASP expression

Intracellular staining with anti-WASP mAb was performed as described by Kawai *et al.* (12) In brief, peripheral blood mononuclear cells (PBMCs) from both a healthy control and the patient were first fixed in 4% paraformaldehyde in PBS for 20 min at room temperature and stained with phycoerythrin (PE)-labeled CD3 (PharMingen, San Diego, CA, USA), CD19 (Beckman Coulter, Fullerton, CA, USA), or CD56 (PharMingen) mAb. Then cells were permeabilized in 0.1% Triton X-100 in Tris-buffered saline (pH 7.4) with 1% fetal calf serum (FCS) and 0.1% NaN_3 for 5 min. Subsequently, these cells were reacted with 10 mg/mL of anti-WASP (5A5) (12) or isotype-matched control mouse IgG2a mAb (PharMingen) for 20 min on ice, washed, and then incubated with 10 mg/mL of fluorescein isothiocyanate (FITC)-conjugated goat anti-mouse IgG2a antibody (Southern Biotechnology Associates, Birmingham, AL, USA). The stained cells were immediately analyzed on an EPICS XL (Beckman Coulter).

Anti-WASP antisera and Western blot analysis

B-Lymphoblatoid cell lines (B-LCLs) were established by inoculating PBMCs from healthy controls and the patient with Epstein–Barr virus (EBV) – containing supernatant (6). B-LCLs from healthy control and the patient were suspended at 1.0×10^7/mL in lysis buffer containing 1% Nonidet P-40, 1 mM phenylmethylsulfonyl fluoride, 0.5% aprotinin, and 10 μg/mL leupeptin at pH 7.5 and were kept on ice for 30 min. From each sample, 40 μg total protein was loaded onto a sodium dodecyl sulfate polyacrylamide gel, electrophoresed, and transferred to a polyvinylidene difluoride (PVDF) membrane (Bio-Rad). The membranes were incubated with rabbit anti-WASP antibody (Ab 503) against a synthetic peptide (aa's 209–226 of WASP) (6) at 1 : 5000 dilutions. The membranes were incubated with alkaline phosphatase-conjugated goat antirabbit immunoglobulin (Promega, Madison, WI, USA). Results were visualized by incubation with AP buffer (100 mM Tris–HCl, pH 9.5; 100 mM NaCl; and 5 mM $MgCl_2$).

DNA purification and sequencing of genomic DNA

Genomic DNA was extracted from the patient's PBMCs using Sepa-Gene (Seikagaku kogyo, Tokyo, Japan). Purified genomic DNA samples were amplified with primer pairs designed to span each exon and exon/intron junction, and the specific causative mutation was identified by direct sequencing as described previously (6). For gene sequencing, informed consent by the patient's family and approval by institutional review boards was obtained.

Patient and results

The patient was the first son of healthy and non-consanguineous Japanese parents, born at term following an uncomplicated pregnancy, and his body weight at birth was 2888 g. His past medical history was unremarkable. At the age of 2 months, he presented with fever, intermittent tachypnea, and general petechiae. On examination, he looked pale and icteric. He had hepatosplenomegaly, but did not have lymphoadenopathy or eczema. Peripheral blood analysis disclosed severe anemia and thrombocytopenia with hemoglobin (Hb) of 3.9 g/dL (normocytic), reticulocytes of 37.8% and platelet count of 11×10^9/L. The mean platelet volume was 5.8–8.1 fL (normal range, 9.0–10.7 fL) and morphology

showed small platelets. White blood cell count (WBC) was 12.3 × 10^9/L. Laboratory investigations revealed the following: serum total bilirubin (T-bil) 3.5 mg/dL (indirect 2.4 mg/dL), lactate dehydrogenase (LDH) 3264 IU/L, aspartate aminotransferase (AST) 210 IU/L, alanine aminotransferase (ALT) 73 IU/L, gamma-glutamyltranspeptidase (γGTP) 257 IU/L, blood urea nitrogen (BUN) 12 mg/dL and creatinine (Cre) 0.22 mg/dL. His prothrombin time, activated partial thromboplastin time and fibrinogen were normal. D-dimer was 7.8 μg/mL (normal range, 0–0.5 μg/mL) and haptoglobin was 8.9 mg/dL with a negative Coombs' test. Furthermore, peripheral blood smears showed fragmented red blood cells. Urinalysis revealed microscopic hematuria.

The patient was diagnosed as having TTP and treated with steroid pulse and plasma exchange (PE) therapy (40 mL/kg/d) for six consecutive days. The patient responded with elevations in the Hb to 8.0 g/dL. LDH decreased to 600 IU/L. Further serum analysis on admission showed a noticeable decrease in ADAMTS13 activity to <0.5% (normal, 70–120%), with the existence of anti-ADAMTS13 IgG autoantibody. Anti-ADAMTS13 IgG autoantibody was evaluated with the chromogenic ACT enzyme-linked immunosorbent assay (ELISA) with the Bethesda method in the Department of Blood Transfusion, Nara Medical University. One Bethesda unit is defined as the amount of inhibitor that reduces the enzymatic activity by 50% of the control value, and values >0.5 U/mL are considered significant (13, 14). Our patient showed markedly decreased ADAMTS13 activity (<0.5%) and tested positive for anti-ADAMTS13 IgG autoantibody (3.6 Bethesda U/mL) at the onset of TTP.

Viral serology study showed a positive result for CMV IgM. CMV was subsequently identified by a urine shell vial culture method and a plasma polymerase chain reaction test for CMV (PCR-CMV) demonstrated significant viremia with 7.0 × 10^5 copies/mL. Administration of intravenous ganciclovir (10 mg/kg/d) was initiated. Gancyclovir therapy was continued until viral loads were stable at around 1000 copies/mL and did not seem to further decline. His platelet counts, however, did not rise and the child required repeated platelet transfusions. A trial of intravenous immunoglobulin (IVIG) as well as a trial of systemic prednisone failed to induce a rise in platelet counts. Antiplatelet antibodies were negative. He also developed several episodes of gastroenteritis due to norovirus and methicillin-resistant *Staphylococcus aureus* (MRSA) bacteremia secondary to soft tissue infection or pneumonia, despite the monthly administration of prophylactic treatment with intravenous immunoglobulin. The presence of thrombocytopenia, small sized platelets, frequent potentially life-threatening infections and autoimmune disease led to the consideration of WAS. WASP expression was examined by flow cytometric analysis of intracellular WASP expression and a reduced expression level was detected (Fig. 1A). Western blot analysis of lysates from the normal control showed that WASP was normally expressed (66 kDa), but a truncated WASP was expressed in the patient (Fig. 1B). Sequencing of WASP genomic DNA identified a one-nucleotide (G) deletion at the position of exon 11, that cause a frameshift, resulting in the generation of a premature stop signal at codon 470 (Fig. 1C and 1D). This mutation has not been previously described. Immunological analysis of peripheral blood revealed normal percentages and numbers of $CD3^+$ T cells (1.35 × 10^9 cells/L), $CD19^+$ B cells (0.85 × 10^9 cells/L) and $CD16^+CD56^+$ NK cells (0.78 × 10^9 cells/L). Analysis of cytolytic activity against K562 target cells demonstrated a normal functional activity of the patient's NK cells compared with that from control.

Discussion

The 502-amino acid protein, WASP, consists of five functional domains: an N-terminal *Drosophila*-enabled/vasodilator-stimulated phosphoprotein homology 1 (EVH1) domain, a basic region (BR), a GTPase-binding domain (GBD), a polyproline-rich region (PRR) and a C-terminal verpolin cofilin homology domains/acidic region (VCA) domain (3) (Fig. 1D). Since the causative gene was first isolated and cloned in 1994(15), various unique mutations have been reported in the WASP gene, spanning all 12 exons. Here, we report a novel WASP gene mutation identified in a Japanese boy, that is, deletion of one nucleotide (G) in exon 11 (1345delG), which leads to a frameshift, resulting in a stop codon at amino acid 470. Most missense mutations are localized to the EVH1 domain, and a mutated WASP often cannot bind to WASP-interacting protein (WIP), leading to defective WASP expression (16). However, since 1345delG mutation causes the partial deletion of WASP in VCA domain, but still maintains an intact EVH1 domain for WIP binding, we can assume that the mutant WASP can bind to WIP and is relatively stable, which protects the truncated WASP from being degraded. But, due to the lack of the VCA area, the truncated WASP cannot combine with the actin-related protein (ARP) 2/3 complex, which plays a key role in cytoskeletal remodeling. WASP, in the active form, binds the ARP 2/3 complex, which gives rise to nucleation of actin filaments at the side of pre-existing filaments, thus creating a branching network of actin at the plasma membrane (8). The activity of the ARP2/3 complex was shown to contribute to a variety of cellular functions, including change of cell shape, motility, endocytosis, and phagocytosis (17).

While many thought that autoimmunity was more common in patients with complete WASP deficiency, recent reports show that autoimmunity can occur in both severe and attenuated cases of the disease (6). Antibody-mediated cytopenias are the most frequent manifestation of autoimmune reactions but various vascular and organ-based autoimmune processes have also been reported (18). Although 22–72% of reported WAS cases suffered from autoimmune disorders,